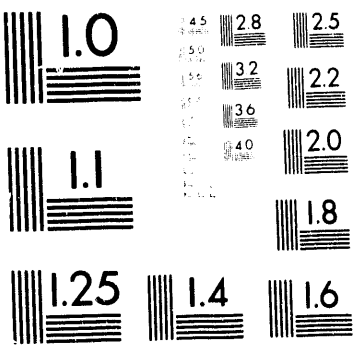
1.0
2.8
2.5
3.2
2.2
3.6
4.0
2.0
1.1
1.8
1.25
1.4
1.6

1 of 1

by a contractor of the U. S. Government under contract No. W-31-109-ENG-38. Accordingly, the U. S. Government retains a nonexclusive, royalty-free license to publish or reproduce the published form of this contribution, or allow others to do so, for U. S. Government purposes.

December, 1990
ANL-HEP-TR-91-13

SDC Hadronic Mass Resolutions in Z and Z′ Decays

DISCLAIMER

This report was prepared as an account of work sponsored by an agency of the United States Government. Neither the United States Government nor any agency thereof, nor any of their employees, makes any warranty, express or implied, or assumes any legal liability or responsibility for the accuracy, completeness, or usefulness of any information, apparatus, product, or process disclosed, or represents that its use would not infringe privately owned rights. Reference herein to any specific commercial product, process, or service by trade name, trademark, manufacturer, or otherwise does not necessarily constitute or imply its endorsement, recommendation, or favoring by the United States Government or any agency thereof. The views and opinions of authors expressed herein do not necessarily state or reflect those of the United States Government or any agency thereof.

R. E. Blair, L. E. Price, and H.-J. Trost

Argonne National Laboratory
Argonne, IL 60439

Patent Cleared by
Patent Department, ANL
RELEASED FOR ANNOUNCEMENT BY
Technical Information Services
Date 4/14/91
David R. Hamrin
Technical Information Services, ANL

ABSTRACT

In order to investigate the performance as a function of calorimeter characteristics, events were simulated in the SDC detector for Z and Z' ($m_{Z'} = 1TeV$) production at two different P_T values (50GeV/c and 500GeV/c). This initial study concentrated on the effects of clustering (including jet fragmentation fluctuations and contributions from underlying events), segmentation and calorimeter energy resolution. These studies were intended to explore the capabilities of the SDC detector for reconstruction of hadronic decays of massive particles (Z mass or greater). We find that detector-independent contributions dominate the mass resolution for the range of parameters being considered by SDC. (Although this study formed the basis for Figures 30-34 presented in the SDC Letter of Intent, an improved fitting strategy was used here and many of the numbers have changed slightly.)

MASTER

DISTRIBUTION OF THIS DOCUMENT IS UNLIMITED

1. Contributions to Mass Resolution

Many contributions to reconstructed mass resolution derive from the physics processes and are independent of the detector parameters. The energy and angular resolutions of jets from Z's and Z''s depend on the production process, which determines the distribution of transverse momenta. Furthermore, the dijet mass resolution depends on the Lorentz boost of the Z's and Z''s. At low p_T we form the invariant mass of the two jets, whereas for highly boosted Z's the invariant mass of the coalesced jet provides the best estimate of the mass. At low p_T, jets are broad, with substantial tails of particles escaping from any reasonable clustering region, while, at high p_T, jets form tighter clusters, and clustering losses are smaller, but still not negligible. For this reason the optimal size for the clustering region depends on the p_T of the jet.

Another dependence on the production process comes from the inevitable inclusion in the clustering region of particles that arise from the underlying event and not from the actual Z or Z'. Fluctuations in this underlying event degrade the energy and angular resolutions. The effect of particles lost from the clustering cone can be reduced by increasing the cone size, but this leads to increased fluctuations in the contribution of the underlying event and other events from the same bunch crossing.

A further contribution to the detector-independent resolution effects arises from fluctuations in the energy fraction carried away by undetected neutrinos from semileptonic decays of heavy quarks inside the jet. These losses produce a long tail of low invariant masses of the dijet system. Finally, gluon radiation also leads to losses out of the clustering cone.

Detector induced resolution effects that have been studied here include:

- calorimeter segmentation,
- calorimeter energy resolution,
- magnetic field and

- nonlinearity of the hadron calorimeter

2. Event Generation

Event samples for two P_T ranges of Z and Z' (mass=$1000 GeV/c^2$) were generated. The low P_T sample extended from 50 to $60 GeV/c$ and the high range extended from 500 to $600 GeV/c$. Events were simulated in the SDC detector as described in the Letter of Intent[1].

Z events were generated using Pythia 4.9 to allow comparison with a previous study done using this same generator for Higgs events. Z's were generated with the Pythia defaults for Z plus jet production, except for the choice of top mass (taken as $100 \mathrm{GeV}/c^2$) and Q_T cuts. The events were presampled to insure that the Z had P_T within the prescribed limits (50 to 60 GeV for one sample and 500 to 600 GeV for the other), and decayed non-leptonically. For most of the study central rapidity ($|\eta| < 1$) was also required to avoid getting only forward production for the low P_T case).

Z' events were generated with similar conditions. The top mass (more important in this case) was set to $150 GeV/c^2$ and the rapidity cut on the initial Z' was relaxed to $|\eta| < 2.5$ since the decay kinematics of the Z' would uominate the jet rapidities of the events.

For both Z and Z' events, the bosons were generated with unique masses, in order to allow study of detector resolution effects with maximum sensitivity. The Z intrinsic width is considerably smaller than than the detector-independent effects studied here. For the Z', the width is model-dependent but with typical values of 0.2-1.4% is also smaller than detector-independent effects[2].

The particles were tracked through the inner part of the detector using GEANT 3.13 through a 2.0 Tesla magnetic field (radius of 1.9 m) up to the calorimeter where the shower spreading was simulated using a parametrization and integration technique implemented in ANLSIM[3]. Data was saved including the Pythia event and the individual depositions of each particle in the calorimeter. The calorimeter

fluctuations and clustering, etc. were then simulated using this same sample of events with different detector configurations and clustering conditions by imposing the fluctuations and non-linearities on the unfluctuated tower depositions.

The event generation was performed on Silicon Graphics systems at Fermilab and SSC lab and on Crays at Florida State and Argonne. The event generation and simulation took about 6 minutes on the Silicon Graphics and 1 to 2 minutes on the Cray's. Typical data samples consisted of 1200 events for Z''s and 600 events for Z's.

3. Clustering Method

Events were clustered using a simple algorithm that selected seed towers in descending order of their energy. Energy within a fixed radius R (in $\eta - \phi$) of the seed tower is gathered for those towers with energy above a single tower threshold and not already associated with a previous cluster. In most cases the value of R was taken as 0.7 and the tower size used was $\Delta\eta = \Delta\phi = 0.05$. This process continued with all available seeds (those not already a part of a cluster) until the energy of the seed candidates fell below a fixed energy minimum. The plots appearing here used a single tower threshold of 0.1 GeV and a seed threshold of 2.0 GeV. Clusters were not saved unless they had more than 5GeV in E_T. The clustering constructed a momentum four vector which used each tower as a massless entry, thus producing a time-like vector.

The final clusters formed in this way are identified as jets. The jet 4-momentum vector is then calculated by summing all calorimetric cells above the tower threshold within the cone, treating each cell as a massless particle. The invariant mass of the two jet system is calculated as $M_{JJ} = [(E_1 + E_2)^2 - (\vec{p}_1 + \vec{p}_2)^2]^{1/2}$. For high p_T Z's, when the two jets have coalesced, we calculate a single jet mass as $M_{JJ} = \sqrt{\mathrm{E}_1^2 - |\vec{p}_1|^2}$.

4. Jet Selection for Mass Reconstruction

Histograms of reconstructed masses from the above procedure are shown in Figures 1a through 1d. In these plots all clusters are used, with no attempt to select likely Z or Z' jets. The two-jet mass distribution is plotted for all samples except the $p_T = 500$ GeV Z sample where the single jet mass distribution is used. The only limitation is that for the Z sample, clusters are required to have at least 15 GeV in E_T and for the Z' plots the jets must have at least 250 GeV of E_T. It is clear that combinatorics play a significant role in determining the shape of these distributions and that in many cases the effective mass resolution will be determined by the presence of "wrong" combinations.

To minimize the influence of the combinatorics and cluster selection, and to allow a better indication of the importance of calorimetry, we have used the event generation information to help in the cluster selection. Several methods were investigated to associate 'clusters' with Z(Z') 'jets', in order to allow a comparison. One method took the information about the initial q and $\overline{q}$ directions and found the closest cluster in direction. If the q and $\overline{q}$ were unresolved (i.e. within a cluster radius of each other) then only one cluster was sought with the resultant direction, otherwise two were chosen. A second method allowed more than one cluster to be associated with the decay products of the Z(Z'). It found all (or any) clusters whose momentum vector (see above) fell within a cluster radius of the quarks.

Finally a modification of the clustering was made to allow the seed to be the 'true' direction of the quarks to facilitate comparisons with this simpler approach. This is an approach used by an independent study at Fermilab which obtains similar results to those quoted here[4].

Differences between these methods were small and were not observed to be systematic within our statistics. We have chosen to report resolutions for the first cluster-choosing method (clusters closest to the quarks) because of its simplicity. We also report a few results for comparison in idealized cases for clustering about the actual quark direction reported by the Monte Carlo program.

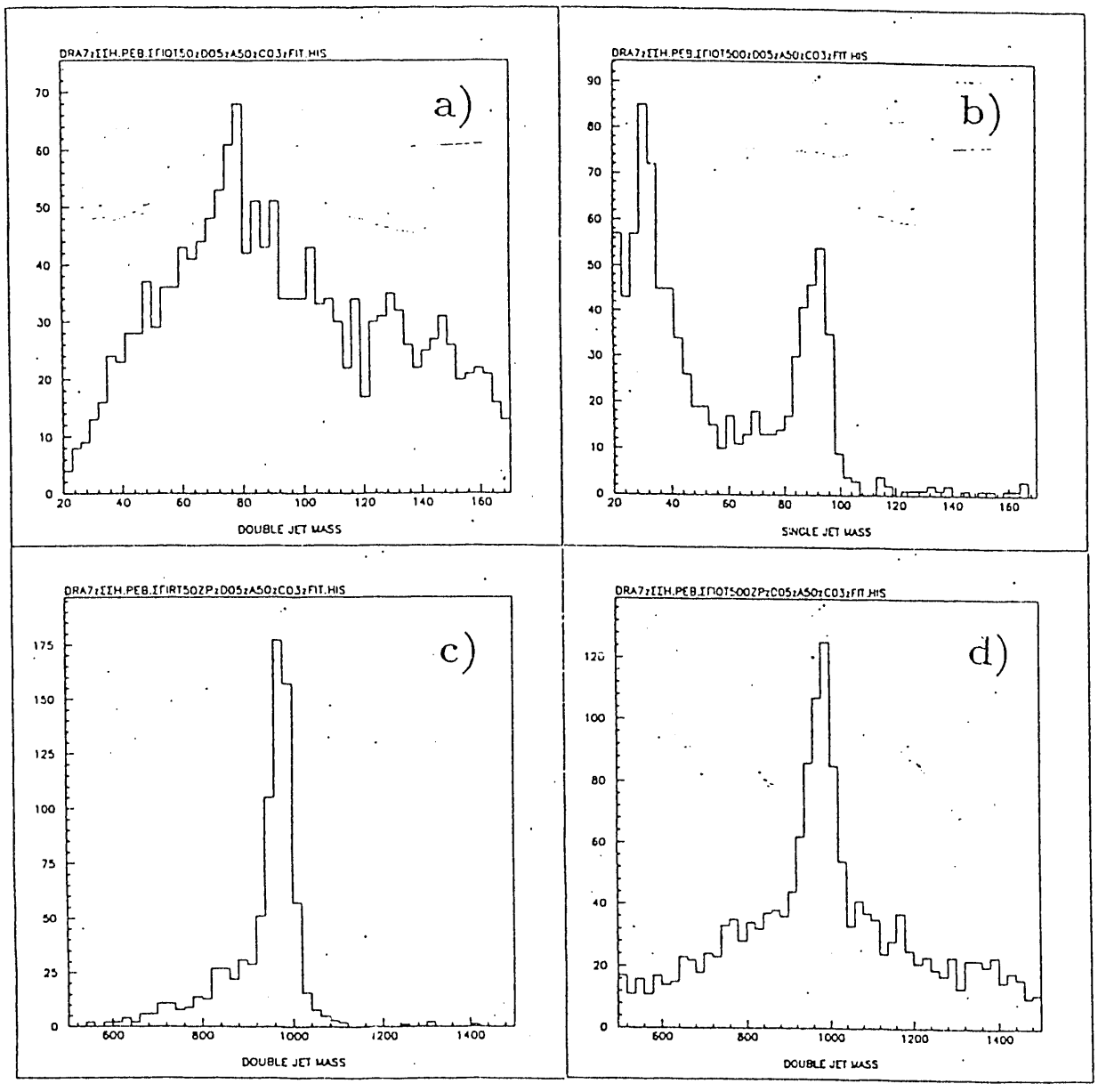

Fig. 1. Reconstructed mass plots for all combinations of clusters. a) Low p_T Z; b) High p_T Z; c) Low p_T Z'; d) High p_T Z'.

5. Results

The mass distributions calculated for any of these methods consists of a Gaussian peak with long asymmetric tails. The tails favor the low mass side with losses arising primarily from undetected neutrinos and from gluon radiation. Contributions to the less populated high mass side come from additional particles from the underlying event falling in the clustering cone. A simple fit to a Gaussian yields unpredictable results when applied to these distributions. The simplest fitting function that could be generally used with satisfactory results consisted of a Gaussian plus a fourth order polynomial. Even this method needed to be guided to a good region of parameters for fitting in order to avoid finding a poor fit in a local minimum of χ^2. The polynomial fit was first performed on the region on the two sides of the peak and then a Gaussian was fit to the distribution that remained after subtracting the polynomial from the peak data.

Figures 2a through 2d show distributions obtained from the clusters closest to the quark directions along with fits made with the above procedure. In these figures, the nominal calorimeter parameters have been used (hadronic resolution given by $0.5/\sqrt{E} \oplus 0.03$ and electromagnetic resolution given by $0.15/\sqrt{E}$ with segmentation $\Delta\eta = \Delta\phi = 0.05$).

Table 1 presents the results of fits to the mass distributions for all four data samples and for a number of detector configurations. The form of the fit was:

$$N(M) = N_{TOTAL}\frac{A_G}{\sqrt{2\pi}\sigma}e^{-(M-M_0)^2/2\sigma^2} + a_0 + a_1 M + a_2 M^2 + a_3 M^3 + a_4 M^4$$

In order to compare resolutions obtained with different conditions, we use the value of σ from the Gaussian part of the fit. The table reports on the Gaussian part of the mass distribution by presenting the values of M_0, σ/M_0 and the error reported by the fitting program on σ/M_0.

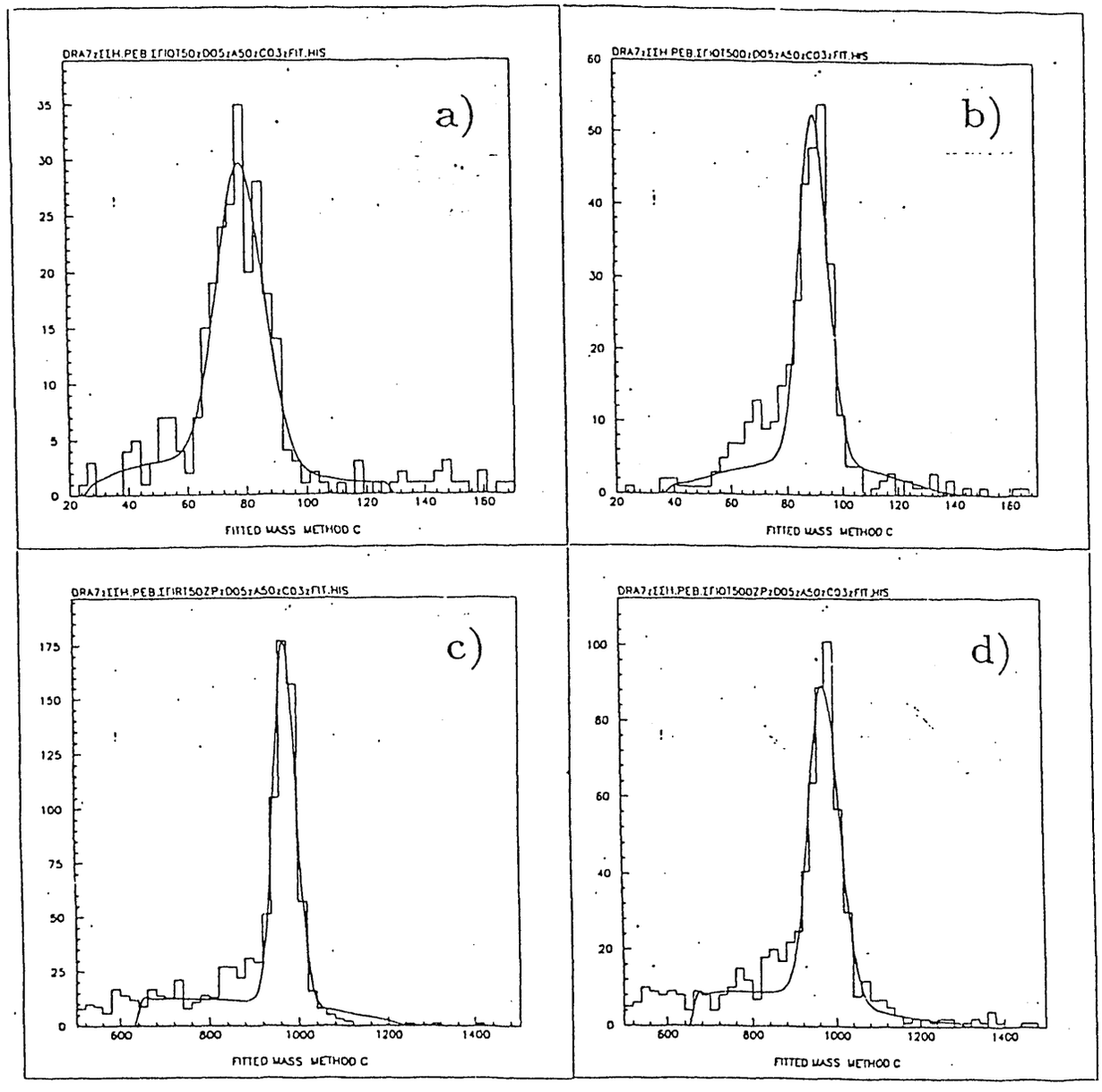

Fig. 2. Same as Fig. 1 but for use of the "correct" choice of clusters only as described in the text.

Table 1

Summary of fitted resolutions. The columns give the particle type (P), either Z or Z', the transverse momentum (p_T), the calorimeter segmentation (s), the hadron calorimeter stochastic coefficient (h_s), and constant term (h_c), the electromagnetic stochastic coefficient (e_s), the clustering radius R, the clustering algorithm C, e/h, fitted peak mass M, and fractional width with fitting error (σ_M/M). The value of C is 'Pythia' for use of particles generated by Pythia for clustering with no calorimeter simulation; 'Quarks' for use of the Pythia quark directions as seeds for clusters of simulated calorimeter towers; or 'Seed' for use of simulated calorimeter towers themselves as seeds for clusters.)

P	p_T (GeV/c)	s	h_s	h_c	e_s	R	C	e/h	M (GeV)	σ_M/M
Z	50	No Cal. Simulation				0.7	Pythia		89.6	0.0289 ± 0.0032
Z	50	.05	0.00	.00	.00	0.7	Quarks	1.0	78.4	0.0830 ± 0.0090
Z	50	.05	0.30	.02	.15	0.7	Seed	1.0	78.6	0.0957 ± 0.0098
Z	50	.05	0.50	.03	.15	0.7	Seed	1.0	78.2	0.1000 ± 0.0073
Z	50	.05	0.70	.04	.15	0.7	Seed	1.0	81.2	0.0970 ± 0.0085
Z	50	.05	1.00	.05	.15	0.7	Seed	1.0	83.6	0.1204 ± 0.0122
Z	50	.05	0.50	.03	.25	0.7	Seed	1.0	78.3	0.0910 ± 0.0073
Z	50	.05	0.50	.03	.15	0.7	Seed	1.3	70.0	0.1034 ± 0.0080
Z	50	.10	0.50	.03	.15	0.7	Seed	1.0	79.3	0.0982 ± 0.0078
Z	50	.15	0.50	.03	.15	0.7	Seed	1.0	80.5	0.0929 ± 0.0073
Z	500	No Cal. Simulation				0.7	Pythia		91.1	0.0192 ± 0.0017
Z	500	.05	0.00	.00	.00	0.7	Quarks	1.0	90.4	0.0515 ± 0.0055
Z	500	.05	0.00	.00	.00	0.7	Seed	1.0	88.9	0.0509 ± 0.0053
Z	500	.05	0.30	.02	.15	0.7	Seed	1.0	89.4	0.0493 ± 0.0055
Z	500	.05	0.50	.03	.15	0.7	Seed	1.0	90.1	0.0558 ± 0.0044
Z	500	.05	0.70	.04	.15	0.7	Seed	1.0	90.8	0.0596 ± 0.0044
Z	500	.05	1.00	.05	.15	0.7	Seed	1.0	92.3	0.0635 ± 0.0050
Z	500	.05	0.50	.03	.25	0.7	Seed	1.0	89.7	0.0662 ± 0.0047
Z	500	.05	0.50	.03	.15	0.7	Seed	1.3	82.1	0.0653 ± 0.0053
Z	500	.10	0.50	.03	.15	0.7	Seed	1.0	91.9	0.0745 ± 0.0082
Z	500	.05	0.50	.03	.15	0.4	Seed	1.0	86.4	0.0514 ± 0.0095
Z	500	.05	0.50	.03	.15	1.0	Seed	1.0	91.7	0.0663 ± 0.0062
Z'	50	No Cal. Simulation				0.7	Pythia		1001	0.0136 ± 0.0007
Z'	50	.05	0.00	.00	.00	0.7	Quarks	1.0	975.0	0.0236 ± 0.0016
Z'	50	.05	0.00	.00	.00	0.7	Seed	1.0	969.7	0.0200 ± 0.0011
Z'	50	.05	0.30	.02	.15	0.7	Seed	1.0	970.9	0.0234 ± 0.0014
Z'	50	.05	0.50	.03	.15	0.7	Seed	1.0	972.6	0.0251 ± 0.0012
Z'	50	.05	0.70	.04	.15	0.7	Seed	1.0	975.9	0.0272 ± 0.0014
Z'	50	.05	1.00	.05	.15	0.7	Seed	1.0	985.4	0.0323 ± 0.0027
Z'	50	.05	0.50	.03	.25	0.7	Seed	1.0	973.0	0.0254 ± 0.0012
Z'	50	.05	0.50	.03	.15	0.7	Seed	1.3	889.8	0.0358 ± 0.0021
Z'	50	.10	0.50	.03	.15	0.7	Seed	1.0	973.2	0.0243 ± 0.0012
Z'	50	.15	0.50	.03	.15	0.7	Seed	1.0	974.6	0.0261 ± 0.0014
Z'	50	.05	0.50	.03	.15	0.4	Seed	1.0	966.6	0.0235 ± 0.0019

Table 1 (Continued)

P	p_T (GeV/c)	s	h_s	h_c	e_s	R	C	e/h	M (GeV)	σ_M/M
Z′	500	No Cal. Simulation				0.7	Pythia		1008	0.0114 ± 0.0007
Z′	500	.05	0.00	.00	.00	0.7	Quarks	1.0	972.9	0.0375 ± 0.0027
Z′	500	.05	0.00	.00	.00	0.7	Seed	1.0	969.4	0.0395 ± 0.0033
Z′	500	.05	0.30	.02	.15	0.7	Seed	1.0	970.5	0.0399 ± 0.0026
Z′	500	.05	0.50	.03	.15	0.7	Seed	1.0	975.6	0.0370 ± 0.0023
Z′	500	.05	0.70	.04	.15	0.7	Seed	1.0	978.5	0.0382 ± 0.0027
Z′	500	.05	0.50	.03	.25	0.7	Seed	1.0	975.7	0.0358 ± 0.0022
Z′	500	.05	0.50	.03	.15	0.7	Seed	1.3	890.3	0.0506 ± 0.0033
Z′	500	.10	0.50	.03	.15	0.7	Seed	1.0	977.7	0.0369 ± 0.0024
Z′	500	.15	0.50	.03	.15	0.7	Seed	1.0	978.9	0.0356 ± 0.0029
Z′	500	.05	0.50	.03	15	0.4	Seed	1.0	975.4	0.0365 ± 0.0043
Magnetic field off:										
Z	500	.05	0.00	.00	.00	0.7	Seed	1.0	88.3	0.0606 ± 0.0036
Z	500	.05	0.50	.03	.15	0.7	Seed	1.0	88.9	0.0613 ± 0.0042
Z	500	.05	0.70	.04	.15	0.7	Seed	1.0	89.7	0.0666 ± 0.0045
Z	500	.05	1.00	.05	.15	0.7	Seed	1.0	91.1	0.0678 ± 0.0047
Z	500	.05	0.50	.03	.25	0.7	Seed	1.0	89.2	0.0616 ± 0.0039
Z	500	.05	0.50	.03	.15	0.7	Seed	1.3	80.4	0.0641 ± 0.0049
Z′	50	.05	0.30	.02	.15	.7	Seed	1.0	962.9	0.0263 ± 0.0043
Z′	50	.05	0.50	.03	.15	.7	Seed	1.0	972.2	0.0286 ± 0.0027
$1.0 < \|\eta\| < 2.5$:										
Z	500	.05	0.50	.03	.15	0.7	Seed	1.0	94.6	0.0641 ± 0.0052

6. Resolution Studies

In Fig. 3 and Fig. 4, we present results from Table 1 on calculations of the dijet mass resolution for a number of assumptions about the detector-independent contributions and about the calorimeter parameters for the Z and Z' at both high and low p_T. The different effects are invoked sequentially in successive points on the graphs in order to demonstrate the different contributions to the dijet resolution. The conditions in the points on the graph are as follows:

(a) The original quark direction is used as the center of a clustering cone of radius 0.7, within which the energy from all detectable tracks in the generated event is combined as a jet. Extra tracks from the underlying event are included. No simulation of showers is performed. This shows the contribution to the mass resolution of basic physics processes, including fluctuations in fragmentation energy outside the cone, effects of the underlying event, missing neutrinos, and gluon radiation.

(b) Our detector simulation distributes the shower energy with a realistic shape, but perfect energy resolution is assumed. Clustering is now done with seed towers as described above. This point represents a minimum resolution for a perfect detector with a reasonable tower geometry.

(c) Same as (b) with the addition of energy resolution in the calorimeter cells of $0.3/\sqrt{E} \oplus 0.02$ for individual hadrons and $0.15/\sqrt{E} \oplus 0.01$ for photons and electrons.

(d) Same as (c) with a hadronic calorimeter resolution of $0.5/\sqrt{E} \oplus 0.03$.

(e) Same as (c) with a hadronic calorimeter resolution of $0.7/\sqrt{E} \oplus 0.04$.

(f) Same as (d) with an electromagnetic calorimeter resolution of $0.25/\sqrt{E}$.

(g) Same as (d) with calorimeter noncompensation corresponding to the extreme limit of the acceptable range considered by SDC, namely $e/h = 1.3$. The resulting overall constant term of about 4% in the hadronic energy resolution is in addition to the 3% constant term introduced in (d) for each hadron. The

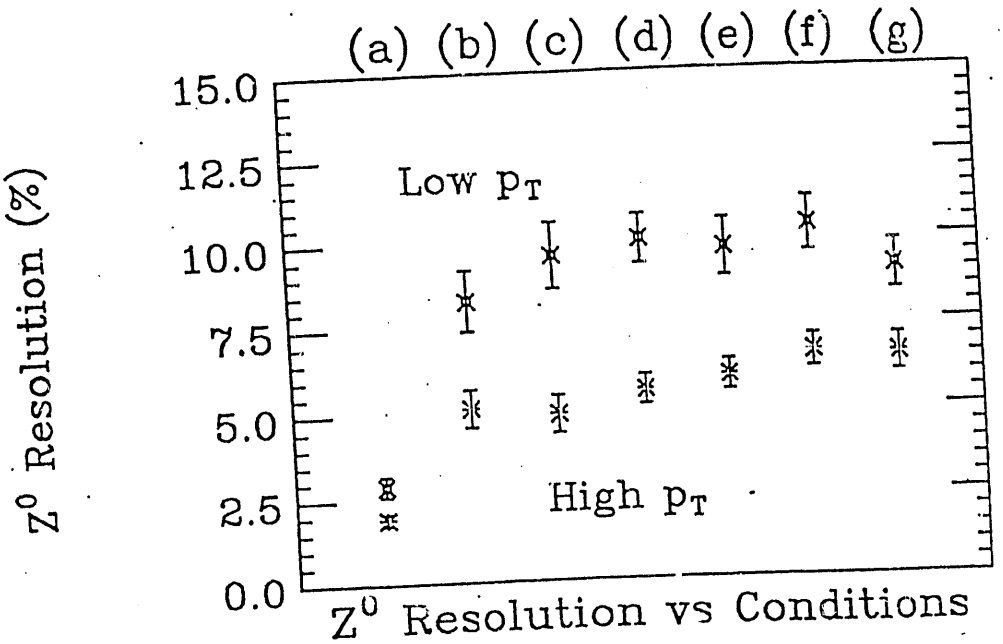

Fig. 3. Summary of mass resolution calculations for reconstructed Z's for the two p_T ranges described in the text. The first two points show the effect of detector-independent contributions to the resolution. The following points show the effect of variations in detector performance. The values plotted represent the sigma from the fits described in the text. The error bars correspond to the statistical error on the sigma. See the text for explanations of each entry.

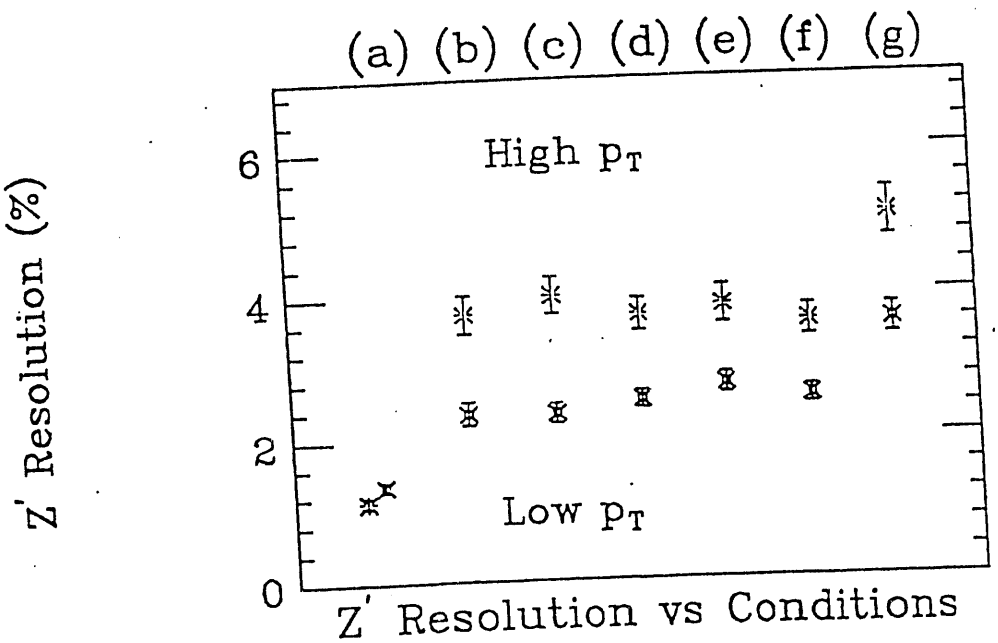

Fig. 4. Same as Fig. 4 but for Z''s of mass 1 TeV.

nonlinear response of the hadron calorimeter due to imperfect compensation is simulated using an ansatz of Groom[5].

In Figs. 3 and 4, the first two points can be understood as successively adding effects that arise from the physics process and the irreducible parts of the measurement process, and do not reflect the specific capabilities of the SDC calorimeter. The remaining points illustrate the effect of calorimeter parameters that span the range of calorimeter performance being considered by the SDC. The dominant contribution to the mass resolution does not come from the detector but from clustering and other effects. In the case of low p_T Z's the mass resolution is dominated by clustering, the fluctuation of energy outside the $R = 0.7$ cone and by fluctuations of the underlying event. A perfect detector can measure the Z mass with a resolution of about 8%. Detector induced effects worsen this resolution by at most a factor of 1.25. In the high p_T Z case, most particles are well contained in the cone and the minimal resolution is about 5%. Detector induced effects may worsen the resolution by about a factor of 1.2. In the case of the Z', the detector-dependent contributions are negligible for high p_T and small for low p_T except for the effect of the extreme e/h value introduced in (g) above, which worsens the resolution by about a factor of 1.5. The Z''s have worse resolution at high p_T than at low p_T because of the larger role played by angular resolution effects.

The effect of hadronic calorimeter resolution is summarized in Fig. 5 for two of the data sets. The horizontal axis of the graph shows the coefficient of the stochastic term in the hadronic resolution with values up to 100%. The constant term is varied along with the stochastic term as shown in Table 1. Over the region of parameters that fall within SDC specifications (30% to 70%) the mass resolution rises by about a factor of 1.2 in each case, while increasing the coefficient to 100% gives a total rise of up to a factor of 1.4.

The segmentation of the calorimeter influences the angular resolution and hence the mass resolution. Previous studies have shown a weak dependence of the mass resolution on segmentation[6]. The effect of calorimeter segmentation is summarized

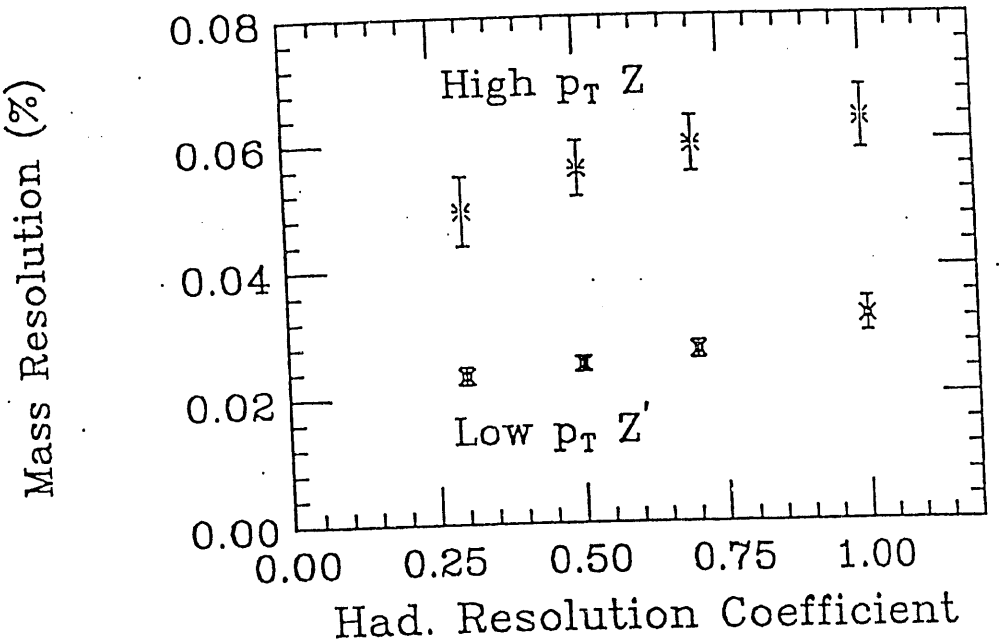

Fig. 5. Reconstructed mass resolutions for high p_T Z and low p_T Z' as a function of hadronic calorimeter resolution. Values are plotted vs the coefficient of the stochastic resolution term, with constant term values tracking the stochastic term as shown in Table 1.

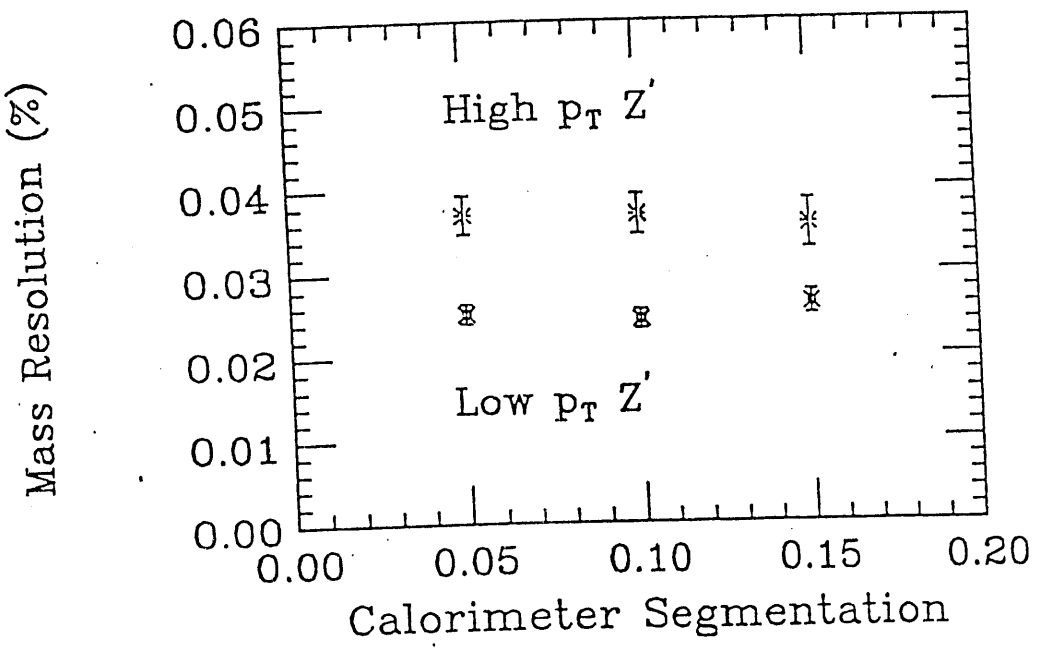

Fig. 6. Reconstructed mass resolutions for high and low p_T Z' as a function of calorimeter segmentation.

in Fig. 6 for the two Z' data sets. In the range up to $\Delta\eta = \Delta\phi = 0.15$, no effect is seen on the mass resolution.

The results presented in the graphs above include the effects of the solenoid field. The magnetic field acts to spread jets, removing some energy from the clustering cone, and also changes the direction of the energy flow within the cone. In order to assess the magnitude of these effects, we have simulated points from two of the data sets with no magnetic field, choosing the better resolution cases for Z and Z'. Approximately a 10% degradation of the mass resolution is seen in each of these cases.

Finally, we have checked the effect of concentrating our calculations in the central $|\eta|$ region, by finding the resolution for high p_T Z's for values of $|\eta|$ from 1.0 to 2.5. Degradation by a factor of 1.15 is seen.

7. Conclusions

We conclude from the results presented here that physics rather than the detector parameters dominates the jet mass resolution over the range considered for SDC. Contributing effects include jet clustering, jet fragmentation uncertainties, and fluctuations in the underlying event. For the best resolutions as limited by physics (those for the Z', the extreme case of $e/h = 1.3$ added to another constant resolution term noticeably degrades the resolution. For calorimeters built with reasonably achievable performance as indicated by recent collider detectors, the jet mass resolution will be as good as the physics allows it to be.

Work supported in part by the U.S. Department of Energy, Division of High Energy Physics, under contract W-31-109-ENG-38.

REFERENCES

1. SDC Letter of Intent, November, 1990
2. I. Hinchliffe, M. L. Mangano, and M. D. Shapiro, SDC-90-00036 (1990)
3. H.-J. Trost, Proceedings of Workshop on Physics and Detector Simulation for SSC Experiments, January, 1990
4. A. Para, *et al.*, SDC-90-00149 (1990)
5. D. E. Groom, "Energy Scaling of Low-Energy Neutron Yield, the e/π Ratio, and Hadronic Response in a Calorimeter," *Proc. of the Workshop on Calorimetry for the Superconducting Super Collider,* Tuscaloosa, Alabama, 13–17 March 1989, ed. R. Donaldson and M. G. D. Gilchriese, World Scientific (June 1990), 59–75
6. J. Freeman and C. Newman-Holmes, in *Experiments, Detectors, and Experimental Areas for the SuperCollider,* p. 673, ed. by R. Donaldson and M. G. D. Gilchriese, Berkeley, CA, 1987 (1988);
   A. Bay *et al.*., in *Proc. of the 1988 Summer Study on High Energy Physics in the 1990's,"* p. 882, ed. by F. J. Gilman and S. Jensen, Snowmass CO, July 1988 (1989).

DATE
FILMED
12/7/93

END